

# MSTAR: Multi-Scale Backbone Architecture Search for Timeseries Classification

Tue M. Cao<sup>1,2</sup>, Nhat H. Tran<sup>1,2</sup>, Hieu H. Pham<sup>\*2</sup>, Thanh Hung Nguyen<sup>1</sup>, and Phi Le Nguyen<sup>1</sup>

<sup>1</sup>Hanoi University of Science and Technology

<sup>2</sup>VinUni-Illinois Smart Health Center, VinUniversity

## Abstract

Most of the previous approaches to Time Series Classification (TSC) highlight the significance of receptive fields and frequencies while overlooking the time resolution. Hence, unavoidably suffered from scalability issues as they integrated an extensive range of receptive fields into classification models. Other methods, while having a better adaptation for large datasets, require manual design and yet not being able to reach the optimal architecture due to the uniqueness of each dataset. We overcome these challenges by proposing a novel multi-scale search space and a framework for Neural architecture search (NAS), which addresses both the problem of frequency and time resolution, discovering the suitable scale for a specific dataset. We further show that our model can serve as a backbone to employ a powerful Transformer module with both untrained and pre-trained weights. Our search space reaches the state-of-the-art performance on four datasets on four different domains while introducing more than ten highly fine-tuned models for each data.

## 1 Introduction

Time Series data (TS) is a sequence of data points recorded or collected at successive points in time. A time series, by nature, can be decomposed into an infinite number of frequencies, each having its own coefficient by novel transformation methods such as Fourier transform, Wavelet transform, etc. Within a particular dataset, each frequency can be identified as either an informative attribute or mere noise based on its significance to the outcomes of a classification model. Consequently, in Time Series Classification (TSC), most methods have developed many flexible ways to extract and differentiate between useful and noisy frequencies. However, due to a wide range of approaches and settings to extract real-world data, time series appears in many different forms, containing various types of signals on various time scales [8, 40, 32]. Furthermore, each dataset prioritizes a distinct set of informative frequencies while disregarding others as noise. Therefore, the primary objective of TSC is to effectively isolate and leverage crucial signals across various time scales while minimizing the impact of insignificant ones.

Several strategies have been formulated to tackle this issue. One primary method is to concentrate on receptive fields [40]. Omni-Scale CNN aims to resolve the dilemma of the optimal receptive fields by introducing a unique architecture that integrates diverse prime-kernel-size convolutions. This design can capture an extensive range of receptive fields, ensuring comprehensive coverage of frequencies across all time scales. However, this approach faces a challenging problem of scaling with larger datasets because of the unique architecture, which comprises only three convolutional layers, limiting the complexity of the feature space that can be explored. Additionally, the use of multiple convolutions within a single layer ( $O(r)/\log(r)$  where  $r$  is the largest receptive field) poses difficulties in scaling, as adding more layers would significantly increase the number of parameters. Expanding the receptive field size to accommodate longer signals may also result in overfitting [40]. Another popular approach is the ensemble of 1-layer convolutions with various kernel sizes and dilations [11, 9, 10, 38] to extract frequencies in a rapid and efficient manner. Despite its innovative nature, this method also suffers from

---

\*Corresponding author.

ineffectiveness when it comes to large data compared to deep learning models [15] as their models are mainly tested on UCR and UEA archive [8, 3] that mostly consist of relatively small or tiny datasets. Other approaches such as [32, 33] leverage different novel transformations that represent time series in more comprehensible ways, and then use a machine learning classifier to label each data point. The state-of-the-art approach, [26], ensembles others’ classifier, which intuitively creates a robust classifier that is proven to be the best method on [8]. All of these techniques also revolve around extracting signals in time series at different scales, but most importantly, they all need to overcome the scalability challenge of a machine learning based approach.

On the other hand, while deep learning models such as Inception Time [20], 1D-ResNet [17], and xResNet [18] exhibit greater adaptability to larger datasets, their ability to capture every size of receptive field is limited by their fixed structures and parameter constraints. Furthermore, although having to manually design the structure of deep learning models, the most critical frequencies for a dataset may not be obvious to researchers and can vary with the type of data. This makes the design more time-consuming, and yet, does not guarantee the optimal architecture for specific datasets. We summarize the shortcomings of previous approaches in Table 1.

Task	Multi-scale	Scalability	Auto design
Deep learning [30, 18, 20]	$X$	$\checkmark$	$X$
OmniScaleCNN [40]	$\checkmark$	$X$	$X$
Others [26, 32, 33, 9, 10, 38, 11]	$\checkmark$	$X$	$\Delta$
MSTAR (our)	$\checkmark$	$\checkmark$	$\checkmark$

Table 1: The overview of previous methods in Time series classification.  $\Delta$  means not relevant.

Lastly, although the main challenge addressed by previous methods to reach state-of-the-art results in TSC is through filtering frequencies [32, 20, 40, 9], we argue that the resolution in the time axis of the extracted frequency significantly influences the predictive accuracy of classification models. Which, to get a better view, we show the relation between receptive field (as well as frequency) and time frame in the state-of-the-art model in section 6.

These mentioned challenges urge us to come up with **MSTAR (Multi-Scale Time series ARchitecture search)**, a deep learning backbone that leverages the multi-scale convolution, drawing inspiration from the Inception-liked models [37, 20] and neural architecture search (NAS) [56]. Our approach of NAS for time series classification suggests a novel way to tackle the formidable problem of architecture manual construction. By employing NAS, our approach aims to search for the optimal range of receptive fields tailored to a specific dataset, which lies at the heart of the successes of other TSC models, and further bring out the architecture that best preserves the time resolution for each critical frequency. We summarize our contributions as below:

- We introduce **MSTAR** as a multi-scale convolutional backbone search space, of which the primary goal is to search for the optimal architecture that is capable of extracting the essential frequencies needed for time series classification. **MSTAR** found 4 completely different architectures that reached state-of-the-art performance at 4 datasets ranging from relatively small (10K) and up to large (1M) at distinct domains compared to many previous TSC approaches.
- We provide a novel framework along with an effective autoencoder that aids our search space to find novel architectures in any dataset.
- We do analytic experiments to show that the time resolution is also a critical factor to be taken into consideration when building TSC models.
- We find that our CNN-backbone can be paired effectively with pre-trained Vision Transformer (ViT) [13] compared with other 1D-CNNs. Allowing our backbone to harness the power of global contextual understanding, as well as leveraging sophisticated pattern recognition offered by large vision models.

## 2 Related works

### 2.1 Time series classification

In the exploration of Time Series Classification (TSC), methods such as [9, 10, 38, 11], have marked significant strides. They utilize convolution without training the weights as the main strategies for frequency extraction in an efficient but robust manner. Other methods such as [32] use symbolic representation to minimize the noise while aiming to enhance signal representation. HIVE-COTE v2 [26] stands out as the state-of-the-art, integrating multiple classifiers for robust performance. However, those mentioned methods predominantly undergo evaluation on smaller datasets from the UCR and UEA archives, highlighting a scalability challenge. Deep learning approaches like InceptionTime [20], TCN [4] and others [30, 18] have better adaptability to larger datasets, offering flexibility and overcoming some limitations of earlier models. Yet they too face challenges in manual design complexity and the architectures may not be suitable for some specific types of datasets.

To alleviate the challenges for deep learning models, Omni-Scale CNN [40] offers an innovative architecture to capture a broad spectrum of frequencies by integrating diverse prime-kernel-size convolutions. This method is adept at ensuring comprehensive coverage across all time scales. However, its scalability is hampered by the architecture’s simplicity, which includes only three convolutional layers. This limitation not only restricts the complexity of the feature space that can be explored but also the model scaling due to the exponential increase in parameters with added layers. Moreover, the risk of overfitting escalates with the expansion of the receptive field to encompass longer signals.

### 2.2 Neural architecture search

Neural architecture search (NAS) is a technique that automates the process of designing and optimizing the architecture of neural networks instead of manually specifying the network’s structure [56]. Prior surveys [14, 48] have pointed out three main components of NAS: search space, search strategy, and performance evaluation strategy.

When it comes to NAS search spaces, they are divided into cell-based [25], chain-based [39], and hierarchical search spaces [7], with cell-based search spaces perhaps being the most popular ones. Cell-based search spaces are inspired by the fact that the most successful CNNs designed with repeated patterns stacked on top of each other, therefore narrowing down the search to only relatively small cells, as opposed to searching the entire network from scratch [56]. This type of search space has significantly lower complexity compared to the other two, making it our choice of design in this paper [48]. In the field of image classification, there have been many search spaces of high quality, such as NAS-Bench-101 [53] and NAS-Bench-201 [12], and inspired by the famous manually designed ResNet [17]. However, to the best of our knowledge, there has been a lack of effective search spaces to encapsulate effective 1D-CNN architectures for the task of time-series data classification. Our novel cell-based search space is built upon the basis of the Inception-liked structure [37, 20], a powerful convolution layer that incorporates multi-scale convolution filters and inception-like blocks to capture diverse temporal patterns.

On the other hand, search strategies have become the main focus of NAS research in recent years. Search strategies can be generally divided into two categories, namely: black box optimization [56, 2, 47] and one-shot technique [25, 29, 5], each of which has its own unique characteristics and advantages over the other. One-shot, which has been prominent in the field of NAS due to its efficiency, has every model in the search space evaluated using the weights from one large model called supernet [25] or hypernet [5]. However, the trustworthiness of not training a model directly has been a debatable topic [48]. Meanwhile, the black box mechanism picks several models by either training from scratch [56] or by using predictors [47]. Algorithms for the construction of architecture batches range from evolutionary and genetic algorithms [2], reinforcement learning [56], Bayesian Optimization [16, 47], etc. Although the black box method usually involves a great requirement of computational resources (due to individual training of many architectures for evaluation), their conceptual simplicity makes them a more accessible option in most applications and this work is no exception. Our approach is inspired by the framework of BANANAS [47] and Bayesian Optimization [16], however, with great modifications to suit our applications.

### 3 Methodology

In this section, we first discuss in more depth the impact of the time resolution of non-trivial frequencies and the reason for the design of our search space in [subsection 3.1](#). Afterward, we will elaborate on the specific detail of the search space and components in the framework in the remaining subsections.

#### 3.1 Motivation

Continuous Wavelet Transform (CWT) has been applied widely in signal processing for AI [\[45, 23, 49\]](#) due to its effectiveness in understanding how the frequency content of the signal evolves over time. In addition, CWT for discrete signals bears great similarities to the convolutional layer in CNNs:

$$CWT_{a,b} = \frac{1}{\sqrt{a}} \sum_{n=0}^{N-1} x[n] \cdot \psi^* \left( \frac{n-b}{a} \right) \quad (1)$$

Where  $x[n]$  is the discrete signal at time  $n$ ,  $\psi^*$  is the complex conjugate of the mother wavelet function,  $a$  and  $b$  are the scale and the translation of the wavelet function respectively. Parameter  $a$  controls the scaling (or frequency) of the mother wavelet while  $b$  handles the translation (or shifting) where it slides the center of the wavelet along the input signal. The combination of both parameters allows capture features at various frequencies and time locations, analyzing non-stationary signals by compromising between time and frequency resolution. Similarly, convolutional layers operate on the principle of local receptive fields, scanning the input signal by shifting the kernel weights along the time axis where these kernel can have different sizes or scales. Previous works have pointed out that convolution kernels often include filters for frequencies [\[22, 54, 55\]](#) where sliding convolution kernel helps remove noise while enhancing useful frequencies. We can view the convolution as a general case of CWT where the kernel’s weights (or wavelet filter) are not determined by mathematical properties but rather constructed from training with the data. Consequently, applying convolutional weights on signals resembles the mechanism of downgrading the time resolution in exchange for extracting frequencies.

Therefore, we contend that TSC should put more weight on the time resolution of the extracted features. This proposition is intuitive, as in certain time series types, the range of beneficial frequencies may vary across different time locations [\[41\]](#). By knowing the exact time frame of the processing frequencies, classification models are provided with critical predictive information that is often overlooked by previous methods [\[40, 9, 10, 11\]](#). Focusing only on the frequency problem, one naive approach would employ very large kernel size convolutions which contain an aggregation of various frequency filters. Based on Fourier analysis that a signal can be decomposed into multiple distinct frequencies, scaling from fine-grained (high frequency) up to the length of the receptive field (low frequency) [Figure 1](#), each acts as a filter to process the input signal [\[34\]](#). In theory, these convolution can capture all of the necessary features, thus, satisfying the frequency extraction requirement. However, this method would not work as the time uncertainty is high for shorter signals (higher frequency) due to the extensive kernels that blur out the precise time locations [\[34\]](#).

We conduct an experiment to verify the claim [Table 2](#). We create five models denoted as  $M_i$  where  $i$  is the length of the extensive convolution kernel, and an additional model  $M_{all}$  which contains a set of distinct kernel sizes scaling from 3 to 20. Other hyperparameters are the same between the models which ensures that they have roughly the same magnitude of the number of trainable weights. The dataset for testing is PTB-XL [\[44\]](#), a popular dataset in electrocardiography (ECG) fields. Further details regarding the experiment are elaborated in [Appendix B](#). As indicated in [Table 2](#), the multi-scale model demonstrates superior performance in classification tasks. In contrast, the other models’ performances gradually decrease as the kernel size gets broader. This implies that the downgrade of time resolution extracted by large convolution leads to the loss of crucial information in TSC. It is important to note that, [\[40\]](#) witnessed the same phenomenon, however, they only discuss about the impact of the receptive fields. We will discuss about the relation between time and receptive fields further in the [section 6](#).

To address the problem, one solution comes naturally. We employ NAS [\[56\]](#) as a novel way to search for an architecture that could be highly finetuned for a specific dataset, where it is chosen to have a unique set of convolutions to capture all beneficial frequencies with the highest time resolutions. In addition,

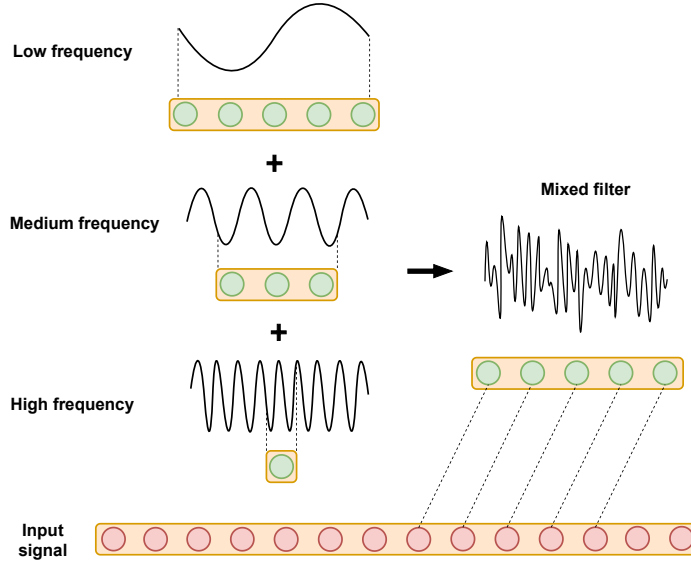


Figure 1: A large kernel, or a complex signal, can be dissected into multiple frequency components. Each component functions as a distinct filter, isolating a specific frequency from the input signals.

Task	$M_{all}$	$M_{20}$	$M_{30}$	$M_{40}$	$M_{50}$	$M_{60}$
Super	<b>0.9325</b>	0.9308	0.9301	0.9275	0.9231	0.9222

Table 2: The comparison of multi-scale model and large-kernel-size models with the "super" task in the PTB-XL dataset. The reported metric is AUC, the best performance is highlighted in bold.

by only selecting necessary frequencies, our search space can avoid having excessive convolutions, thus, having better scalability than previous multi-scale approach [40] shown in section 5. Our design for the search space is inspired by Inception-like architectures [37, 20] which favor a "wide" convolutional layer over "deep" like ResNet [17]. Due to the great flexibility of Inception, our search space can construct various models that, by stacking convolution form a wide range of receptive fields [37], allowing extraction of frequencies across multiple time scales.

### 3.2 Search Space

We constructed a cell-based search space that can be represented with a graph as shown in Figure 2. The graph includes 13 nodes  $\{N_i \mid i \in 0, \dots, 12\}$  partitioned into 3 layers, the first node and the last node (which have the indexes of 0 and 12) are the input node and output node respectively. The first layer contains node 1 ( $N_1$ ), the second contains 5 nodes from node 2 ( $N_2$ ) to node 6 ( $N_6$ ), the last layer consists of node 7 ( $N_7$ ) to node 11 ( $N_{11}$ ). Each node has an attribute of the number of channels, denoted as  $C_i$ , which indicates the number of output channels of that node, the initial channel size of each node is provided in Figure 2. As shown, there are two types of channels: 128 and 32, the former is the standard channel size of a node while the latter serves as a bottleneck channel size (based on InceptionTime) which minimizes the computational complexity of the model.

The edge that connects a pair of nodes denoted as  $E_{ij}$  symbolizes one of the predefined operations namely: convolution, max pooling, average pooling, and identity. The output of nodes with smaller indexes will be forwarded to the respective operation and transformed into the output of nodes with larger indexes. For example, if  $N_i$  and  $N_j$  are connected and  $i < j$ , the output of  $N_i$ , which has  $C_i$  channels, will be passed through an operation stored in edge  $E_{ij}$  to become the output of node  $N_j$  having the channel of  $C_j$ . Furthermore, the channel of each node will be determined by the minimum channel of all the previous nodes (nodes with smaller indexes) that are connected to it, and nodes within the same layer cannot be wired together. Lastly, nodes that are not connected to any upper layers' node will be transformed to have the default of 128 channels (by concatenating with other

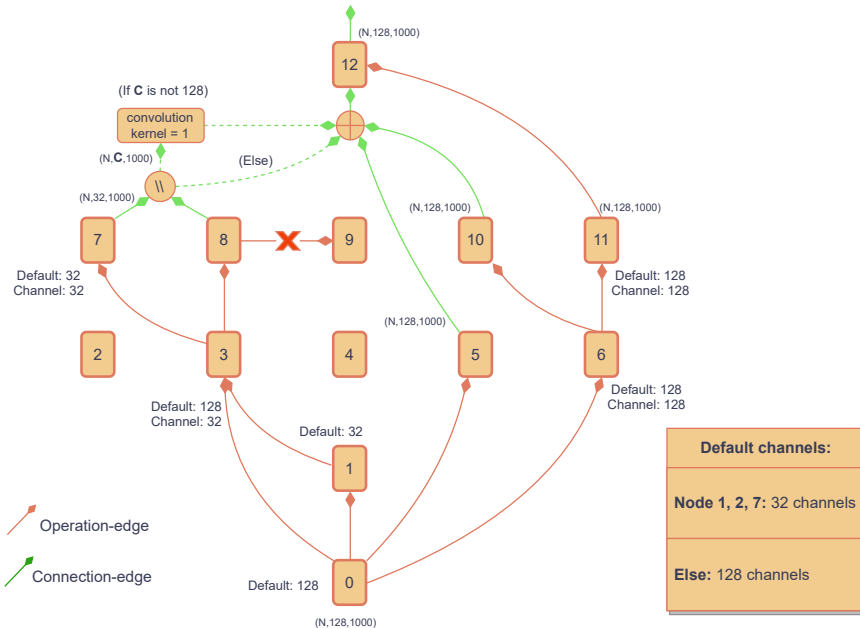


Figure 2: search space’s cell visualization: The default channel sizes along with the preprocessed channel sizes are provided. Edges that connect 2 nodes are denoted as operation-edge (orange) and contain an operation, other edges are used purely for connection (green).

bottleneck nodes and passing through depth-wise convolution) and then added to the output of the last node to be forwarded to the next cell. An example is provided in Figure 2.

In the search space, kernel sizes are selectable for different operations. Specifically, for convolution, the default sizes are 1, 3, 5, 9, 19, and 39, while for max and average pooling, the options are 3, 5, and 9. This choice of kernel sizes, which is inspired from previous TSC model InceptionTime [20], allows our search space to construct multiple receptive fields by stacking convolutions [37], providing flexibility in extracting necessary frequencies while maintaining reasonable time resolution. Ultimately, the model is formed by assembling multiple identical cells and can either be attached with a classifier for classification or serves as a backbone for time series processing.

### 3.3 Search space encoding

A model can be represented by its unique cell, we encoded our search space with a  $4 \times 13 \times 13$  matrix denoted as  $A \in \mathbf{A}$  which is concatenation of four  $13 \times 13$  adjacency matrices for each operation, with each element in an adjacency matrix indicates the connection between a pair of nodes. Specifically, if  $N_i$  and  $N_j$  are wired together then  $A[i, j]$  contains the kernel size of the operation ( $A[i, j] = 1$  for the Identity), if  $N_i$  and  $N_j$  are not connected then  $A[i, j] = 0$ . An illustration can be found in Figure 3.

### 3.4 Framework

We will discuss in details about the framework in this section. The overall framework is inspired by the BO neural predictor of BANANAS [47], we use Bayesian Optimization (BO) [16] to search for superior models at each iteration. The acquisition function is defined as the Expected Improvement (EI) where the mean and variance are derived from calculating the mean and variance of the outputs of a group of predictors. These predictors are trained to predict the performance of a given model.

We first pre-train an autoencoder on the search space so that it could capture and project the adjacency matrix to the vector space  $\mathbf{V}$ . Furthermore, we initialize a population by training a set of  $N$  models that were generated randomly  $P_{init} = \{label_i : A_i \mid i = 1, 2, \dots, N_{init}\}$ . A set of predictors, denoted as  $Preds = \{p_i, \mid i = 1, 2, \dots, N_{preds}\}$ , is trained on the initial population over  $E_p$  epochs. This

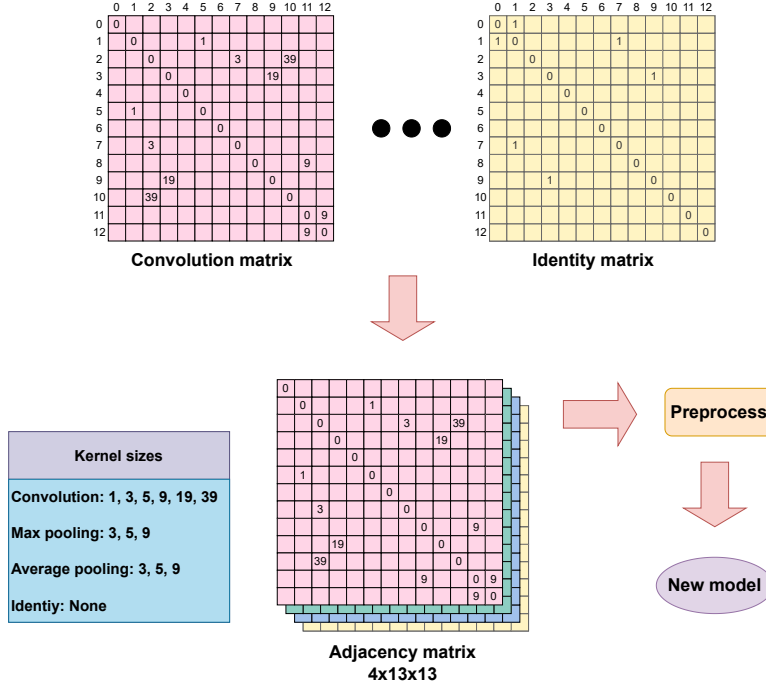


Figure 3: search space’s encoding visualization: The search space can be represented as a  $4 \times 13 \times 13$  Adjacency matrix ( $A$ ). This matrix then will be preprocessed to meet the criteria of the search space.

training involves processing adjacency matrices via the autoencoder’s encoder to derive representations within the  $\mathbf{V}$  space, serving as inputs for the predictors,  $Preds : V \mapsto label$ . At each iteration, the predictors are periodically retrained with the current population for a limited number of epochs to prevent overfitting. Subsequently, a provisional population,  $P_{temp} = \{label_i^t : A_i^t, |, i = 1, 2, \dots, N_{temp}\}$ , is assembled by selecting  $K$  top-performing architectures from the current population and applying mutation operations at a predetermined probability. To maintain a balance between exploration and exploitation, this process is complemented by the introduction of newly generated models into  $P_{temp}$ . Each model within this temporary population is then processed through the encoder,  $Encoder : \mathbf{A} \mapsto \mathbf{V}$ , and evaluated by the predictors. The top  $Q$  models are then trained from scratch to determine their true performance labels. These models are subsequently integrated into the main population pool. The pseudo code of the framework is shown in subsection 3.4. It is important to note that throughout this search process, the pre-trained autoencoder remains fixed, and only the encoder component is utilized.

---

**Algorithm 1** Pseudo code of the framework

---

**Require:** pre-trained autoencoder  $CAE$  with the search space

**Require:**  $P_{init} = \{label_i : A_i | i = 1, 2, \dots, N_{init}\}$

- 1: Train predictor  $Preds = \{p_i | i = 1, 2, \dots, N_{preds}\}$  with  $P_{init}$  for  $E_p$  epochs
  - 2: Load and freeze the weights of  $CAE$
  - 3:  $Population = P_{init}$
  - 4: **while** epoch  $< E_s$  **do**
  - 5:   Train  $Preds$  for  $e_p$  epochs on  $Population$
  - 6:   Draw out  $K$  models from  $Population$
  - 7:   Sample  $P_{temp}$  by **randomly generate or mutate** from  $K$  best models in  $Population$
  - 8:   Feeding  $A_i \in P_{temp}$  to the encoder to get the vector  $v_i \in \mathbf{V}$
  - 9:   Pass  $v_i$  through  $Preds$  and **calculate the acquisition function**
  - 10:   Train from  $Q$  highest score models and add to  $Population$
  - 11: **end while**
-

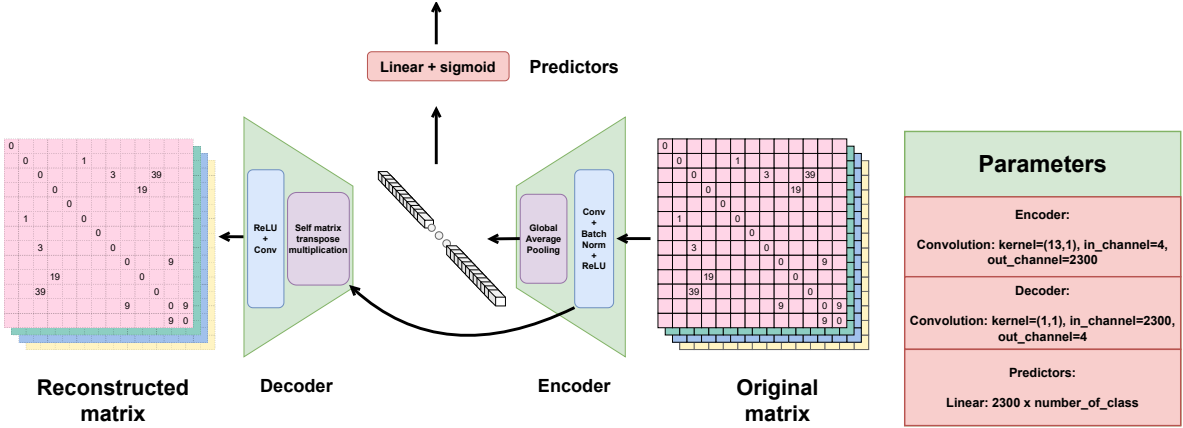


Figure 4: The architecture of our convolutional autoencoder  $CAE$  and predictors.

### 3.4.1 Autoencoder and predictors

Our search space is represented in the form of a  $4 \times 13 \times 13$  matrix which is the same format as an image, hence, we propose an autoencoder denoted as  $CAE$  with convolutional layer Equation 2 and global average pooling (GAP) so that it converts the matrix to a vector space  $v_i \in \mathbf{V}$  that contains information about the model Equation 3. The role of the decoder is to help the encoder create a vector space, projecting from discrete to continuous space, that retains enough information so that the original adjacency matrix can be reconstructed by the decoder Equation 4. In addition to the autoencoder, we use a simple linear layer for the implementation of the predictors. The predictors take the output of the encoder (vector in the vector space  $\mathbf{V}$ ) and feed through a linear layer with sigmoid as the activation function to predict the labels of the processing models Figure 4. Using both autoencoder and predictors prove to have a significant impact on the performance of the predictors compared to only using predictors, which we analyze in detail in section 6.

$$O = ReLU(BatchNorm(Conv(A))) \quad (2)$$

$$v_i = GAP(O) \quad (3)$$

$$\hat{A} = Decoder(O) = ReLU(Conv(OO^T)) \quad (4)$$

## 4 Experiments

### 4.1 Datasets

We conduct our experiments on four datasets at four distinct domains, namely: electrocardiography (ECG), electroencephalography (EEG), human activity recognition (HAR), and satellite image time series (SITS).

#### 4.1.1 PTB-XL

The PTB-XL dataset [44] is a large-scale electrocardiography (ECG) dataset that contains 21,837 clinical 12-lead ECGs from 18,885 patients, recorded between October 1989 and June 1996. These records include extensive annotations by cardiologists, conforming to the SCP-ECG standard, and cover diagnostic, form, and rhythm statements for a comprehensive array of cardiac conditions. The dataset is sampled at both 100 Hz and 500 Hz with a length of 10 seconds, however, we follow [35, 6] and only process the former.

The dataset was split into ten folds, with the tenth fold recommended as the test set and the remaining nine folds as training and validation sets. Following this, we used the first eight folds for training, the ninth fold for validation, and the tenth fold for testing. Moreover, we also use the bandpass filter to remove outlier frequencies, allowing the frequencies in the range of 3-45Hz only, following [6].

The evaluating task is "super-diagnosis" (super) as it is recorded with the least fluctuation in the performances of the models [6]. The main metric for this dataset is AUCROC.

#### 4.1.2 EEGEyeNet

The EEGEyeNet [21] dataset provides a unique combination of high-density electroencephalography (EEG) and eye-tracking (ET) data from 356 healthy adults aged between 18 and 80 years. The dataset was recorded using a 128-channel EEG system and an infrared video-based ET system, both at a sampling rate of 500 Hz. It includes data from three experimental paradigms designed to explore the intersection of brain activities and eye movements. Annotations include the start and end times of saccades, fixations, and blinks, as well as the position of saccades and average position of fixations.

We use the task "absolute position" similar to [52], which is the hardest task according to [21] and contains about 35000 data points. The data is split into three parts with the proportion of 70-15-15 for training, validating, and testing respectively, which is recommended by the benchmark [21]. The metric used for this task is RMSE.

#### 4.1.3 Smartphone HAR

The smartphone HAR [31] is recorded from 30 volunteers aged 19 to 48, who performed six different activities: walking, walking upstairs, walking downstairs, sitting, standing, and lying. These activities were recorded while each participant wore a Samsung Galaxy S II smartphone, sampling at a rate of 50Hz. The raw sensor signals underwent preprocessing to remove noise and were segmented using sliding windows of 2.56 seconds with a 50% overlap, resulting in 128 readings per window.

The dataset contains 10300 data points. We implement the split of 5-2-3 for our experiments with the test data as the default provided by [31]. We follow [50] which adopts  $F_{1-micro}$  as the main metric.

#### 4.1.4 Satellite

The dataset [28] is derived from images taken by the Formosat-2 satellite gathered at Toulouse area in France. These images are multi-channel, allowing for the observation of land cover changes across several years. Each pixel within the images corresponds to a specific geographic area. The primary objective of using this satellite imagery is to create land cover maps that aid in geographical surveying. This involves analyzing sequences of pixels within a particular color channel to classify them into one of 24 different land cover categories.

We utilize the preprocessed data from [42], which contains 1M data points and split into three part with the percentages of 80%, 10%, and 10% for training, validating, and testing respectively. The main reported metric is accuracy.

## 4.2 Setups

The following hyperparameters are constant throughout the experiments. The autoencoder is trained with 800k randomly generated models, with the split of 792k for training and 8k for testing and the learning rate of  $1 \times e^{-2}$  for 100 epochs. The more models used to pre-train the better, however, we chose 800k as the autoencoder showing no further noticeable improvement when we increased the number of models.  $L_2$  loss is utilized for the pre-train of autoencoder which evaluates the distance between real and reconstructed adjacency matrices. We initializes  $N_{init} = 400$  models then trains the  $N_{preds} = 10$  predictors on  $P_{init}$  for  $E_p = 200$  epochs with  $L_2$  loss and learning rate of  $1 \times e^{-3}$ . The framework runs for  $E_s = 50$  iterations. In each iteration, the predictors are trained for  $e_p = 10$  epochs on the current population. The probability of mutation is 0.8 which modifies 15% of the original adjacency matrix. Other hyperparameters are set as follow:  $K = 4$ ,  $N_{temp} = 24$ , and  $Q = 4$ . More details about training models for each dataset can be found in the [Appendix A](#).

## 5 Main results

After each run, our population consists of 600 different models and we draw out the top 10 with the most promising score for evaluation. The best architecture is chosen by averaging throughout five runs and then selecting the highest performance. Our results are presented in the following subsections.

### 5.1 PTB-XL

We conducted an experiment on the "super-diagnosis" task within the PTB-XL dataset, as detailed in Table 3. Our backbone architecture incorporates both average and max pooling layers alongside a standard linear classifier, in line with the structure proposed by [20]. To ensure a balanced evaluation, we scaled the number of parameters in various renowned Time Series Classification (TSC) models, including [40, 4, 30], to match our model's scale. This normalization allows for a more equitable comparison. The presented results encapsulate the average outcomes of five distinct runs.

It is observed that our model surpasses the state-of-the-art performance by a noticeable margin. Other Inception-like models' performances vary significantly. Specifically, IncepSE [6] was the previous best model reaching 0.9343, while XceptionTime performs poorly in the PTB-XL. This shows the flexibility of Inception models which could be exploited to create models that are highly tuned to a specific task. Furthermore, our model exhibits a greater adaptability for larger dataset compared to other receptive-field-based approaches [40, 4], illustrating the need for precise time location rather than focusing on only frequency.

Models	AUC	Parameters
XceptionTime [30]	0.8949	1.5M
TCN [4]	0.9309	1.7M
OmniScaleCNN [40]	0.9191	1.7M
xResNet [18]	0.928	-
ResNet1D-Wang [46]	0.930	-
InceptionTime [20]	0.921	-
ST-CNN-GAP-5 [1]	0.9318	-
IncepSE [6]	0.9343	1.1M
MSTAR (Our)	<b>0.9355</b>	2.3M

Table 3: The AUCROC in super-diagnosis task on PTB-XL.

### 5.2 Satellite

For this dataset, we also evaluate popular TSC models with the number of parameters scaled Table 4. The reported results are the mean after five runs. We chose a linear classifier without any pooling for our backbone CNN as it has a superior outcome compared to other classifiers. Our experiment reveals that, for larger datasets, our model consistently has better performance. MSTAR found a model that exceeds receptive-field methods significantly, outperforming OmniScaleCNN [40] and TCN [4] by 7,7% and 3% respectively. The same trend happens when other Inception-like models' adaptability greatly fluctuates, however, this time, XceptionTime [30] exhibits a more dominant performance. Once again, this implies the potential for a highly tuned Inception model for a specific time series dataset that has yet to be discovered.

### 5.3 Smartphone HAR

Following [50], we report the top-1  $F_{1-micro}$  out of 10 runs and include their results. In alignment with our previous approach, we meticulously calibrated the number of parameters in renowned TSC models

Models	Accuracy	Parameters
XceptionTime [30]	88,7	9.6M
TCN [4]	86,0	10.7M
OmniScaleCNN [40]	85,9	12.0M
xResNet34-deeper [18]	88,0	9.1M
ResNet1D [17]	86.6	-
InceptionTime [20]	84,8	-
MSTAR (Our)	<b>89.0</b>	12.0M

Table 4: The accuracy of TSC models on Satellite.

to a uniform scale, ensuring a fair and balanced comparison. Table 5 demonstrates the adaptation of our search space on a relatively small dataset. Our discovered model surpasses the previous state-of-the-art [50] in the human activity recognition task. This accomplishment underscores the robustness of our framework, particularly in scenarios characterized by limited data availability.

Models	$F_{1-micro}$	Parameters
XceptionTime [30]	0.934	3.5M
TCN [4]	0.876	2.2M
OmniScaleCNN [40]	0.932	1.7M
xResNet19-deep [18]	0.931	5.0M
DeepConvLSTM [27]	0.910	-
InnoHAR [17]	0.945	-
InceptionTime [20]	0.944	1.8M
MSTAR (Our)	<b>0.953</b>	3.7M

Table 5: The  $F_{1-micro}$  on Smartphone HAR.

## 5.4 EEGEyeNet

Finally, we show that our model can be used as a backbone for transformer [43]. We follow previous works on the dataset [21, 52] where the means of RMSE metric are reported after 5 runs. [52] point out that, Vision transformer (ViT) [13] can be paired effectively with CNN. Furthermore, the pre-trained weight of ViT provides an essential pattern recognition mechanism, which substantially enhances the ability of the hybrid model (ViT2EEG [52]) to predict the eye gaze position. We also use ViT and pre-trained ViT for this experiment while using MSTAR and InceptionTime [20] as the backbone. InceptionTime is chosen for its similarity to our model in terms of the overall macro structure as an Inception-like architecture, suitable for a backbone. Moreover, we conduct two separate NAS runs for pre-trained and base ViT respectively and the best models in both categories are reported. The hyperparameters for the pre-trained ViT are the same between each backbone in this experiment. Note that our contribution is not to provide the best result as we could utilize more advanced ViT-based models or use tuned hyperparameters for ViT. Instead, our intention is to demonstrate the ability of our backbone CNN to perform well on tasks other than classification and the flexibility to work with transformers. The results in Table 6 show that both models, MSTAR-ViT-base and MSTAR-ViT-pre-trained, surpass the previous state-of-the-art by substantial margins. Notably, our base model (without pre-trained weights) exceeds the pre-trained EEGViT, further underscoring the potential of using our backbone with transformers.

We also evaluate the performance of InceptionTime as a backbone CNN. Although the impact of VIT on the base model is limited compared to InceptionTime, the weights of VIT trained on image data boost the performance of InceptionTime-VIT-pre-trained significantly. This could be that the InceptionTime is not suitable to be a backbone but the pre-trained weights, with crucial additional information, support a strong performance.

Models	RMSE
Naive	123,3
XceptionTime [30]	78,7
PyramidalCNN [21]	73,9
InceptionTime [20]	70,7
InceptionTime-VIT-base	69,5
InceptionTime-VIT-pre-trained	54,2
VIT-base [13]	61,5
VIT-pre-trained [13]	58,1
EEGVIT [52]	61,7
EEGVIT-pre-trained [52]	55,4
MSTAR-VIT-base (Our)	<b>53,3</b>
MSTAR-VIT-pre-trained (Our)	<b>51,3</b>

Table 6: The results on the EEGEyeNet dataset. The numbers of parameters are not presented because most of the results are concluded from [52, 21].

## 6 Ablation study

We believe that two problems should be discussed further in this section. The first problem is the impact of receptive fields on the frequency and time precision. Moreover, we provide proof of the importance of accurately identifying time to the performance of our TSC model. Secondly, we focus on the effect of using CAE compared to the prominent Variational Autoencoder (VAE) and the accuracy of our predictor.

### 6.1 Receptive fields and time resolution

We first calculate the receptive fields of each node in our state-of-the-art model on the dataset PTB-XL Table 7. Afterward, we visualize the time and frequency of the feature maps in each node via the spectrograms generated by CWT. The results are presented in Figure 5 where we show the spectrogram at layers 1, 2, and 6 of the last 6 nodes excluding the output node. These nodes were chosen because each of them contains a distinct range of receptive fields. At first glance, the plot contains multiple figures that all have vertical dark color stripes, which is expected as ECG is periodical and the stripes mean no heart pulse. At the first layer, it is observed that the broader the receptive fields span, the less rigorous the stripes are. In contrast, larger receptive fields mean stronger frequency intensities, this is indicated by the brighter color. Specifically,  $N_6$  only has the receptive field of 1, which means its feature maps are the most similar to the ECG signal with distinctive stripes and high time resolution. While  $N_7$  contains more and broader receptive fields, hence the range of frequencies captured is wider and stronger but the precision regarding time is degraded. This aligns with our motivation subsection 3.1. Furthermore, the same pattern happens with the next layers. As we dive deeper, the receptive fields get much larger and more complex, which results in the downgrade of time resolution and the features are more abstract as the stripes have been blurred out. It is worth noting that, the nodes with modest receptive fields in the lower layer still have small receptive fields compared to other nodes at the higher

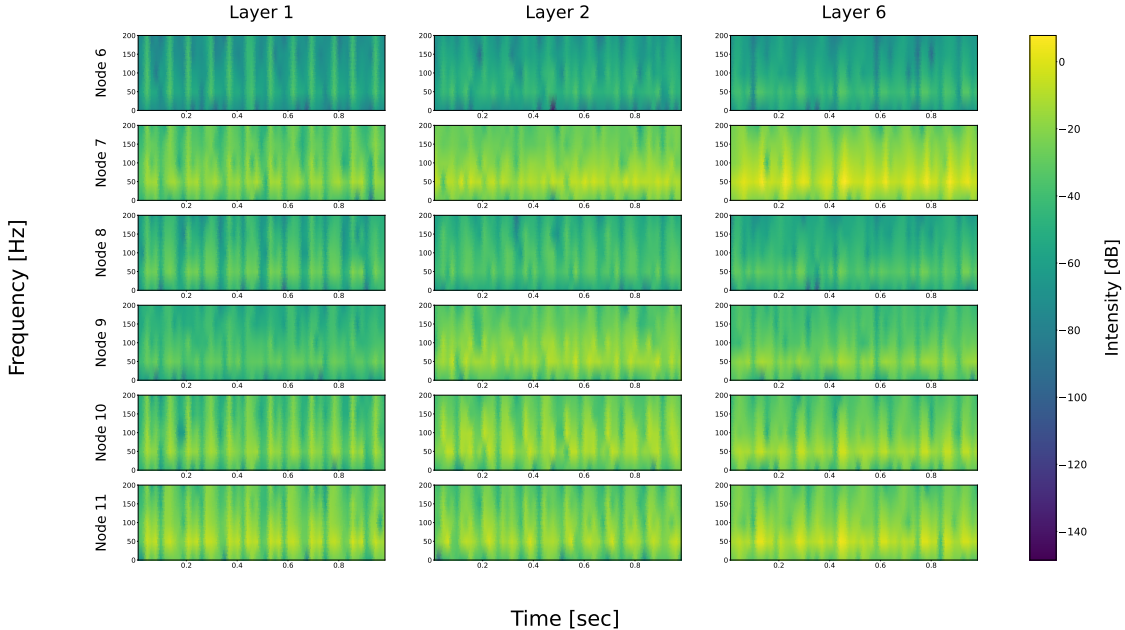


Figure 5: Spectrograms of the feature maps created by Continuous Wavelet Transform (CWT) from MSTAR’s model on PTB-XL [44]. The larger the receptive field, the stronger the frequency intensities. However, this is the trade-off for time resolution.

layer. Thus, the rank, in terms of brightness of the feature maps (indicating the magnitude of the frequencies) within the set of nodes, is still the same for every layer.

Node	Receptive fields
1	Not connected
2	1
3	1
4	9
5	9
6	1
7	1, 3, 17, 27, 39
8	1, 3, 9
9	3, 9
10	1, 3, 5, 9, 11
11	1, 9, 17

Table 7: The receptive fields of every node at the first layer of our MSTAR model on PTB-XL.

We show the importance of time resolution in the first layer in Figure 6. Layer 1 is chosen because of its clear distinction regarding time while still having a variety of ranges of receptive fields. We evaluate the contributions by taking the mean of  $L_1$  norm of the scores for the output of each node given by Integrated Gradient [36], all while zeroing out other nodes. The higher the scores, the greater the contributions to the overall classification. The results in Figure 6 show that the first five nodes have significant gradient quality, which is expected as they also serve as the skip-connection. But most importantly, the last five nodes ( $N_7$  to  $N_{11}$ ), although having different contributions among the classes, none of the contributions can be disregarded. This implies that both time and frequency resolution are essential to our model, providing critical information for classification.

Lastly, with the prior knowledge of the rank in terms of time resolution still remaining the same at each layer, we remove nodes from the adjacency matrix to see their impacts on the performance of our

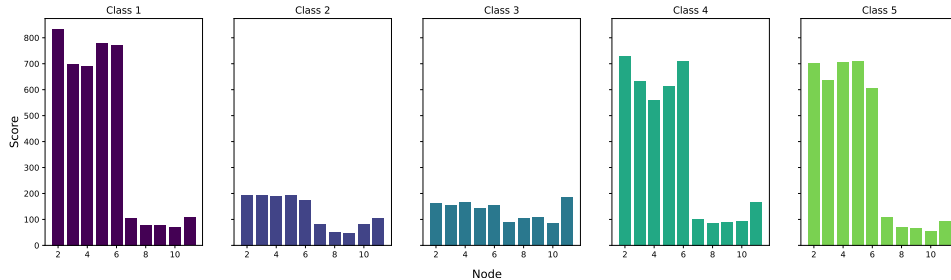


Figure 6: The scores of the nodes in layer 1 from MSTAR’s model on PTB-XL with Integrated Gradient [36]. None of the node has a neglectable contribution.

model. We zero out several nodes that deliver the most accurate time view, which includes  $N_8$ ,  $N_9$ , and  $N_{10}$ . We do not select  $N_6$  as it serves as the skip connection to the model and would already have an important role anyway. In contrast,  $N_7$  and  $N_{11}$  are included in our experiment, as they are among the most critical nodes in terms of frequency resolution, for the sake of comparison. Furthermore, discarding these nodes would not change the structure of another node because they are at the last layer in the cell besides the output node, hence, would not affect the performance if it is not important. Table 8 shows that without the information of precise time location, our model performs noticeably worse, commensurable with the loss of AUC of removing  $N_7$  and  $N_{11}$ . This further implies the essential of time resolution in TSC.

Removing node	$N_7$	$N_8$	$N_9$	$N_{10}$	$N_9$ and $N_{10}$	$N_{11}$
AUC	0.9326	0.9338	0.9352	0.9350	0.9332	0.9345

Table 8: The performances of our model when removing  $N_8$ ,  $N_9$ , and  $N_{10}$  respectively when comparing with  $N_7$  and  $N_{11}$ . Our model is trained from scratch, the mean AUC is recorded after 5 runs.

## 6.2 Impact of autoencoder

The utilization of autoencoder has been proved to have a significant impact on various frameworks [51]. However, different search spaces, that have unique representations, require specific types of autoencoder. Consequently, we show that our Convolutional Autoencoder (CAE) is more suitable than the popular counterpart Variational Autoencoder (VAE). We start by constructing a VAE, of which architecture is demonstrated in Appendix B. The standard  $L_2$  with  $KL$  divergence are adopted as the loss function of the VAE. Furthermore, both of the autoencoders are trained with the setups referred in subsection 4.2 which ultimately evaluate the performance by the  $L_2$  metric. The results are presented in Table 9.

Autoencoder	CAE	VAE
MSE Loss	5.389	14.202

Table 9: The  $L_2$  loss of both autoencoders on 8K randomly initialized adjacency matrices. The CAE is better at reconstructing our search space representation.

We also show the performance of our predictors in measuring the performances of models based on the adjacency matrices. We conduct an experiment with our standard CAE and 10 predictors that compare with modified predictors. These predictors are integrated with a Convolutional block with a pooling layer at the stem so that they can effectively process the matrices. We also make modifications so that the new predictors would reach their best potential as shown in Appendix B. The comparison is shown in Table 10. The Spearman correlation coefficient is adopted as the main metric. We randomly initialize 800 models and train them from scratch across all 4 datasets. We then split with the proportion of 9-1 for training, and validation respectively. The results demonstrate that the pre-trained CAE boosted the accuracy of the predictors substantially, essential for our framework to search on different time series datasets.

Method	CAE and linear predictors	Convolutional predictors
smartphone HAR	0.730	0.382
PTB-XL	0.528	0.246
Satellite	0.321	0.156
EEGEyeNet	0.242	0.238

Table 10: The effectiveness of our autoencoder on the precision of the neural predictors measured in Spearman Correlation. The baseline is random guessing which has the correlation of zero.

## 7 Conclusion

### 7.1 Future works

Our research can be reproduced for follow-up works. We encourage improvements in the framework to improve the efficiency and accuracy of the search. Moreover, another promising direction is to incorporate more advanced operations such as convolution with dilation and groups or the squeeze and excitation module [19]. Lastly, our approach to integrating transformer is still naive, we believe this topic could spark many renovating ideas, and open more possibilities in TSC.

### 7.2 Conclusion

In this study, we propose a multi-scale search space that comes with a novel framework to search for the optimal architecture as well as receptive field range for time series datasets. Our proposed MSTAR backbone overcomes the formidable scalability challenges, leveraging automated searching without human intervention and accomplishing optimistic results. Our experiments reveal that while frequency extraction is crucial, time resolution also plays an important role, providing valuable information in the TSC field. We believe that these findings could provide a broader view of time series processing, incorporating larger models to tackle more extended datasets.

## 8 Acknowledgements

This research is supported by the VinUni-Illinois Smart Health Center, VinUniversity.

## References

- [1] Atul Anand, Tushar Kadian, Manu Kumar Shetty, and Anubha Gupta. Explainable ai decision model for ecg data of cardiac disorders. *Biomedical Signal Processing and Control*, 75:103584, 2022.
- [2] Noor Awad, Neeratyoy Mallik, and Frank Hutter. Differential evolution for neural architecture search, 2021.
- [3] Anthony J. Bagnall, Hoang Anh Dau, Jason Lines, Michael Flynn, James Large, Aaron Bostrom, Paul Southam, and Eamonn J. Keogh. The UEA multivariate time series classification archive, 2018. *CoRR*, abs/1811.00075, 2018.
- [4] Shaojie Bai, J. Zico Kolter, and Vladlen Koltun. An empirical evaluation of generic convolutional and recurrent networks for sequence modeling, 2018.
- [5] Andrew Brock, Theodore Lim, J. M. Ritchie, and Nick Weston. Smash: One-shot model architecture search through hypernetworks, 2017.
- [6] Tue Cao, Nhat Tran, Le Nguyen, Hung Nguyen, and Hieu Pham. Incepse: Leveraging inception-time’s performance with squeeze and excitaion mechanism in ecg analysis. In *Proceedings of the 12th International Symposium on Information and Communication Technology, SOICT ’23*, page 578–584, New York, NY, USA, 2023. Association for Computing Machinery.
- [7] Aristeidis Christoforidis, George Kyriakides, and Konstantinos Margaritis. A novel evolutionary algorithm for hierarchical neural architecture search, 2023.

- [8] Hoang Anh Dau, Anthony J. Bagnall, Kaveh Kamgar, Chin-Chia Michael Yeh, Yan Zhu, Shaghayegh Gharghabi, Chotirat Ann Ratanamahatana, and Eamonn J. Keogh. The UCR time series archive. *CoRR*, abs/1810.07758, 2018.
- [9] Angus Dempster, François Petitjean, and Geoffrey I. Webb. Rocket: exceptionally fast and accurate time series classification using random convolutional kernels. *Data Mining and Knowledge Discovery*, 34(5):1454–1495, July 2020.
- [10] Angus Dempster, Daniel F. Schmidt, and Geoffrey I. Webb. Minirocket: A very fast (almost) deterministic transform for time series classification. In *Proceedings of the 27th ACM SIGKDD Conference on Knowledge Discovery & Data Mining*, KDD '21, page 248–257, New York, NY, USA, 2021. Association for Computing Machinery.
- [11] Angus Dempster, Daniel F. Schmidt, and Geoffrey I. Webb. Hydra: Competing convolutional kernels for fast and accurate time series classification. *Data Min. Knowl. Discov.*, 37(5):1779–1805, may 2023.
- [12] Xuanyi Dong and Yi Yang. Nas-bench-201: Extending the scope of reproducible neural architecture search, 2020.
- [13] Alexey Dosovitskiy, Lucas Beyer, Alexander Kolesnikov, Dirk Weissenborn, Xiaohua Zhai, Thomas Unterthiner, Mostafa Dehghani, Matthias Minderer, Georg Heigold, Sylvain Gelly, et al. An image is worth 16x16 words: Transformers for image recognition at scale. *arXiv preprint arXiv:2010.11929*, 2020.
- [14] Thomas Elsken, Jan Hendrik Metzen, and Frank Hutter. Neural architecture search: a survey. *J. Mach. Learn. Res.*, 20(1):1997–2017, jan 2019.
- [15] Navid Mohammadi Foumani, Lynn Miller, Chang Wei Tan, Geoffrey I. Webb, Germain Forestier, and Mahsa Salehi. Deep learning for time series classification and extrinsic regression: A current survey, 2023.
- [16] Peter I. Frazier. A tutorial on bayesian optimization, 2018.
- [17] Kaiming He, Xiangyu Zhang, Shaoqing Ren, and Jian Sun. Deep residual learning for image recognition. *CoRR*, abs/1512.03385, 2015.
- [18] Tong He, Zhi Zhang, Hang Zhang, Zhongyue Zhang, Junyuan Xie, and Mu Li. Bag of tricks for image classification with convolutional neural networks. *CoRR*, abs/1812.01187, 2018.
- [19] Jie Hu, Li Shen, Samuel Albanie, Gang Sun, and Enhua Wu. Squeeze-and-excitation networks, 2019.
- [20] Hassan Ismail Fawaz, Benjamin Lucas, Germain Forestier, Charlotte Pelletier, Daniel F. Schmidt, Jonathan Weber, Geoffrey I. Webb, Lhassane Idoumghar, Pierre-Alain Muller, and François Petitjean. Inceptiontime: Finding alexnet for time series classification. *Data Min. Knowl. Discov.*, 34(6):1936–1962, nov 2020.
- [21] Ard Kastrati, Martyna Beata Płomecka, Damián Pascual, Lukas Wolf, Victor Gillioz, Roger Wattenhofer, and Nicolas Langer. Eegeyenet: a simultaneous electroencephalography and eye-tracking dataset and benchmark for eye movement prediction, 2021.
- [22] Alex Krizhevsky, Ilya Sutskever, and Geoffrey E. Hinton. Imagenet classification with deep convolutional neural networks. *Commun. ACM*, 60(6):84–90, may 2017.
- [23] Hyeon Kyu Lee and Young-Seok Choi. Application of continuous wavelet transform and convolutional neural network in decoding motor imagery brain-computer interface. *Entropy*, 21(12):1199, 2019.
- [24] Lightning-AI. Pytorch lightning, 2024.
- [25] Hanxiao Liu, Karen Simonyan, and Yiming Yang. Darts: Differentiable architecture search, 2019.

- [26] Matthew Middlehurst, James Large, Michael Flynn, Jason Lines, Aaron Bostrom, and Anthony Bagnall. Hive-cote 2.0: A new meta ensemble for time series classification. *Mach. Learn.*, 110(11–12):3211–3243, dec 2021.
- [27] Francisco Javier Ordóñez and Daniel Roggen. Deep convolutional and lstm recurrent neural networks for multimodal wearable activity recognition. *Sensors*, 16(1), 2016.
- [28] François Petitjean, Jordi Inglada, and Pierre Gancarski. Satellite image time series analysis under time warping. *IEEE Transactions on Geoscience and Remote Sensing*, 50(8):3081–3095, 2012.
- [29] Hieu Pham, Melody Y. Guan, Barret Zoph, Quoc V. Le, and Jeff Dean. Efficient neural architecture search via parameter sharing, 2018.
- [30] Elahe Rahimian, Soheil Zabihi, Seyed Farokh Atashzar, Amir Asif, and Arash Mohammadi. Xceptiontime: Independent time-window xceptiontime architecture for hand gesture classification. In *ICASSP 2020 - 2020 IEEE International Conference on Acoustics, Speech and Signal Processing (ICASSP)*, pages 1304–1308, 2020.
- [31] Reyes-Ortiz, Jorge, Anguita, Davide, Ghio, Alessandro, Oneto Luca, Parra, and Xavier. Human activity recognition using smartphones. UCI Machine Learning Repository, 2012.
- [32] Patrick Schäfer. The boss is concerned with time series classification in the presence of noise. *Data Min. Knowl. Discov.*, 29(6):1505–1530, nov 2015.
- [33] Ahmed Shifaz, Charlotte Pelletier, François Petitjean, and Geoffrey I. Webb. TS-CHIEF: A scalable and accurate forest algorithm for time series classification. *CoRR*, abs/1906.10329, 2019.
- [34] Steven W. Smith. *The scientist and engineer’s guide to digital signal processing*. California Technical Publishing, USA, 1997.
- [35] Nils Strodthoff, Patrick Wagner, Tobias Schaeffter, and Wojciech Samek. Deep learning for ecg analysis: Benchmarks and insights from ptb-xl. *IEEE Journal of Biomedical and Health Informatics*, 25(5):1519–1528, 2021.
- [36] Mukund Sundararajan, Ankur Taly, and Qiqi Yan. Axiomatic attribution for deep networks, 2017.
- [37] Christian Szegedy, Vincent Vanhoucke, Sergey Ioffe, Jonathon Shlens, and Zbigniew Wojna. Rethinking the inception architecture for computer vision. *CoRR*, abs/1512.00567, 2015.
- [38] Chang Wei Tan, Angus Dempster, Christoph Bergmeir, and Geoffrey I. Webb. Multirocket: Multiple pooling operators and transformations for fast and effective time series classification. *Data Min. Knowl. Discov.*, 36(5):1623–1646, sep 2022.
- [39] Mingxing Tan, Bo Chen, Ruoming Pang, Vijay Vasudevan, Mark Sandler, Andrew Howard, and Quoc V. Le. Mnasnet: Platform-aware neural architecture search for mobile, 2019.
- [40] Wensi Tang, Guodong Long, Lu Liu, Tianyi Zhou, Michael Blumenstein, and Jing Jiang. Omniscale CNNs: a simple and effective kernel size configuration for time series classification. In *International Conference on Learning Representations*, 2022.
- [41] Larisa G. Tereshchenko and Mark E. Josephson. Frequency content and characteristics of ventricular conduction. *Journal of Electrocardiology*, 48(6):933–937, 2015.
- [42] Renbo Tu, Nicholas Roberts, Mikhail Khodak, Junhong Shen, Frederic Sala, and Ameet Talwalkar. NAS-bench-360: Benchmarking neural architecture search on diverse tasks. In *Thirty-sixth Conference on Neural Information Processing Systems Datasets and Benchmarks Track*, 2022.
- [43] Ashish Vaswani, Noam Shazeer, Niki Parmar, Jakob Uszkoreit, Llion Jones, Aidan N. Gomez, Lukasz Kaiser, and Illia Polosukhin. Attention is all you need, 2023.
- [44] Patrick Wagner, Nils Strodthoff, Ralf-Dieter Boussejot, Dieter Kreiseler, Fatima I Lunze, Wojciech Samek, and Tobias Schaeffter. Pt看xl, a large publicly available electrocardiography dataset. *Scientific data*, 7(1):154, 2020.

- [45] Tao Wang, Changhua Lu, Yining Sun, Mei Yang, Chun Liu, and Chunsheng Ou. Automatic eeg classification using continuous wavelet transform and convolutional neural network. *Entropy*, 23(1):119, 2021.
- [46] Zhiguang Wang, Weizhong Yan, and Tim Oates. Time series classification from scratch with deep neural networks: A strong baseline, 2016.
- [47] Colin White, Willie Neiswanger, and Yash Savani. BANANAS: bayesian optimization with neural architectures for neural architecture search. *CoRR*, abs/1910.11858, 2019.
- [48] Colin White, Mahmoud Safari, Rhea Sukthanker, Binxin Ru, Thomas Elsken, Arber Zela, Debadepta Dey, and Frank Hutter. Neural architecture search: Insights from 1000 papers, 2023.
- [49] Baoguo Xu, Linlin Zhang, Aiguo Song, Changcheng Wu, Wenlong Li, Dalin Zhang, Guozheng Xu, Huijun Li, and Hong Zeng. Wavelet transform time-frequency image and convolutional network-based motor imagery eeg classification. *Ieee Access*, 7:6084–6093, 2018.
- [50] Cheng Xu, Duo Chai, Jie He, Xiaotong Zhang, and Shihong Duan. Innohar: A deep neural network for complex human activity recognition. *IEEE Access*, 7:9893–9902, 2019.
- [51] Shen Yan, Yu Zheng, Wei Ao, Xiao Zeng, and Mi Zhang. Does unsupervised architecture representation learning help neural architecture search?, 2020.
- [52] Ruiqi Yang and Eric Modesitt. Vit2eeg: Leveraging hybrid pretrained vision transformers for eeg data, 2023.
- [53] Chris Ying, Aaron Klein, Esteban Real, Eric Christiansen, Kevin Murphy, and Frank Hutter. Nas-bench-101: Towards reproducible neural architecture search, 2019.
- [54] Jason Yosinski, Jeff Clune, Yoshua Bengio, and Hod Lipson. How transferable are features in deep neural networks? In *Proceedings of the 27th International Conference on Neural Information Processing Systems - Volume 2*, NIPS’14, page 3320–3328, Cambridge, MA, USA, 2014. MIT Press.
- [55] Matthew D. Zeiler and Rob Fergus. Visualizing and understanding convolutional networks. In David Fleet, Tomas Pajdla, Bernt Schiele, and Tinne Tuytelaars, editors, *Computer Vision – ECCV 2014*, pages 818–833, Cham, 2014. Springer International Publishing.
- [56] Barret Zoph and Quoc V. Le. Neural architecture search with reinforcement learning, 2017.

## A Training setups

Our detailed training setups are presented as follows [Table 11](#). Note that for smartphone HAR, the  $F_{1-micro}$  fluctuated widely and the size of the dataset is limited, hence, we evaluate the architectures for NAS by randomly segmenting the data into 5 folds and implementing 5-fold testing. Moreover, we use Pytorch Lightning API trainer [\[24\]](#) with the learning rate of  $1e^{-3}$  and implement stochastic weight averaging with  $1e^{-4}$  learning rate while running NAS. The setups to evaluate every model after NAS (including our model) in [Table 5](#) are presented in [Table 11](#). For other datasets, we employ training and validating on the default training and validating set, the test set is utilized to evaluate after we run the architecture search for a fair comparison. The training for the remaining datasets is the same throughout the search and benchmarking.

## B Hyperparameters

### B.1 Multi-scale experiment

We create six models with multiple scales as described in [subsection 3.1](#). The hyperparameters of all the architectures are the same and are inspired by InceptionTime [\[20\]](#), which includes five layers with 128 channels, each layer contains the standard convolution, batch normalization, and ReLU as the activation. We use both global average and global max pooling and a linear layer as the classification.

Setups	lr	Optimizer	Scheduler	Population - Datasets	Loss - Criterion	Others parameters
Autoencoder pre-trained	$1e^{-2}$	Adam	OneCycle:	792K - 8K (models)	$L_2$ loss	Epochs:100 Batchsize: 256
Predictors x 10 pre-trained	$1e^{-3}$	Adam	None	$P_{init}$ (400 models)	$L_2$ loss	Epochs: 200 Batchsize: 16
Predictors x 10 each Iteration	$1e^{-3}$	Adam	None	$Population$	$L_2$ loss	Epochs: 10 Batchsize: 16
PTB-XL training	$1e^{-2}$	AdamW	OneCycle	PTB-XL	Binary cross entropy	Epochs: 18 Batchsize: 128
EEGEyeNet training	$1e^{-3}$	Adam	OneCycle	EEGEyeNet	$L_2$ loss	Epochs: 30 Batchsize: 128
Smartphone HAR training	$1e^{-4}$	AdamW	OneCycle	Smartphone HAR	Cross entropy	Epochs: 30 Batchsize: 128
Satellite training	$2e^{-3}$	AdamW	OneCycle	Satellite	Cross entropy	Epochs: 12 Batchsize: 1024

Table 11: The training setups

## B.2 VAE and convolutional predictor

The architecture of the VAE that we build for [subsection 6.2](#) is shown in this section. [Equation 5](#) and [Equation 6](#) show the information flow of our encoder, where  $A_j$  is the adjacency matrix of the  $j$ th operation. The hidden representation at layer  $i$  is denoted as  $H_i$ , it can be further split into four parts  $\{H_{i,j} | j \in \{1, ..4\}\}$  at the last dimension, carry global information of other operations when multiplying with  $A_j$ . The MLP consists of linear, batch normalization, and a leaky ReLU activation function. We chose the leaky ReLU and also the overall architecture because they are the best setups in our empirical experiments. The representation in  $\mathbf{V}$  is derived from  $V \sim \mathcal{N}(\mu, \sigma^2)$  where  $\mu$  and  $\sigma$  are acquired from feeding the last  $H$  through two linear layers respectively. On the other hand, the decoder is described in [Equation 7](#) and [Equation 8](#) where  $\hat{A}$  is the reconstructed matrix.

$$H_0 = \sum_{j=0}^3 A_j W_{encoder} \quad (5)$$

$$H_{i+1} = MLP(Concat_j((1 + \epsilon)H_i + A_j H_{i,j})) \quad (6)$$

$$Z_j = V W_{decoder} \quad (7)$$

$$\hat{A} = ReLU(Concat_j(Z_j Z_j^T)) \quad (8)$$

The convolutional predictor is constructed by using a simple block, which includes convolution, batch normalization, global average pooling, and several feed-forward layers with tanh activation. This architecture resembles the combination of our CAE and linear predictor. The hyperparameters of both VAE and predictor are tuned so that they leverage the best performances. For the variational autoencoder, we implement five layers with a hidden dimension of 128 and the MLP contains two linear layers. The predictors have 2300 channels for convolution (same as the CAE) and contain four feed-forward layers with the number of neurons decreasing by half each layer, starting with 2300.